

Spin-Crossover Behaviors of Iron(III) Compounds with Strong Intermolecular Interactions

Shinya Hayami,*[1] Soushi Miyazaki,[1] Masahiko Yamamoto,[1] Kenji Hiki,[1] Natsuko Motokawa,[1] Aya Shuto,[1] Katsuya Inoue,[2] Teruo Shinmyozu,[3] and Yonezo Maeda[1]

[1]Department of Chemistry, Faculty of Science, Kyushu University, 6-10-1 Hakozaki, Higashi-ku, Fukuoka 812-8581

[2]Department of Chemistry, Faculty of Science, Hiroshima University, 1-3-1 Kagamiyama, Higashi-hiroshima 739-8526

[3]Institute for Materials Chemistry and Engineering, Kyushu University, 6-10-1 Hakozaki, Higashi-ku, Fukuoka 812-8581

Received July 12, 2005; E-mail: hayascc@mbox.nc.kyushu-u.ac.jp

Iron(III) spin-crossover compounds with H3-OMe-salRen ligands $[Fe(3\text{-}OMe\text{-}salRen)_2]ClO_4$ (**1**–**5**) were prepared and characterized by single-crystal X-ray diffraction, Mössbauer spectra, magnetic susceptibilities, and electronic spectra, where 3-OMe-salRen is a tridentate ligand derived from 3-methoxysalicylaldehyde and *N*-R-ethylenediamine (R = H, Me, Et, Pr, and Bu for **1**, **2**, **3**, **4**, and **5**). The structures of compounds **1**, **2**, **3**, and **5** at 90 and 298 K, and that of compound **4** at 298 K were determined. Compounds **1**, **2**, **3**, and **5** exhibited a spin transition depending on temperature; the transition temperatures for **1**, **2**, **3**, and **5** were >400, 360, 196, and 223 K, respectively. Compound **4** was in the high-spin state in the temperature range of 5 to 400 K. σ–π or π–π interactions exist in compounds **1**–**5**, and the structures of the compounds were made clear in both the high-spin and low-spin states. Compound **3** exhibited a spin transition with thermal hysteresis.

The design of molecules that could be utilized for information processing and information storage is one of the main challenges in molecular materials science. Molecules that would be suitable for such applications must exhibit bistability, which can be defined as the property of a molecular system that allows it to exist in two different electronic states over a certain range of external perturbation. A typical example of a molecular species that exhibits such a molecular bistability is spin-crossover compounds. Since the discovery of the first spin-crossover compound,[1] a variety of d^n ($n = 4$–7) transition-metal compounds exhibiting bistability between the high-spin (HS) and low-spin (LS) states have been reported.[2] Usually, the spin-transition phenomena can be induced by a variation of temperature, pressure, or magnetic field.[3,4] On the other hand, Decurtins et al. showed that the spin transition could be induced by illumination in 1984.[5] This finding shows that spin-crossover compounds have potential applications as optical switches and data storage devices.[5,6]

The spin-crossover phenomenon depends strongly on intermolecular interactions.[7] When the magnitude of these intermolecular interactions overcomes the threshold value, the spin-crossover phenomenon becomes cooperative. In such a case, the spin transitions between the LS and HS states may not only be very abrupt, but may also occur with a hysteresis effect. The presence of the hysteresis effect is important, because a molecular compound that exhibits hysteresis can take two different electronic states between $T_{1/2}\uparrow$ and $T_{1/2}\downarrow$ depending on its history, enabling the fabrication of information storage and processing devices. Note that $T_{1/2}\uparrow$ and $T_{1/2}\downarrow$ are defined as the temperatures for which there are 50% HS and 50% LS states in the warming and cooling modes, respectively. A compound with a large thermal hysteresis at room temperature needs to be developed for practical applications.[8] Although many attempts have been made to produce a suitable compound in previous studies, so far the production of spin-crossover compounds with such a wide hysteresis has been a challenging issue.[9–11] Hendrickson et al. reported that the series of spin-crossover iron(III) compounds $[Fe(X\text{-}salEen)_2]Z$ (X = H, 3-OMe, 4-OMe, 5-OMe, and 3-OEt; Z = NO_3, PF_6, and BPh_4) exhibited most all of the curiosities observed for spin-crossover compounds in the solid state.[12] Only the compound $[Fe(3\text{-}OMe\text{-}salEen)_2]PF_6$ in the series of compounds exhibited an abrupt spin transition, and we focused on this compound, because compounds exhibiting abrupt spin transitions show large cooperativity and bistability. Here, we show that the mononuclear iron(III) compounds, $[Fe(3\text{-}OMe\text{-}salHen)_2]ClO_4$ (**1**), $[Fe(3\text{-}OMe\text{-}salMen)_2]ClO_4$ (**2**), $[Fe(3\text{-}OMe\text{-}salEen)_2]ClO_4$ (**3**), $[Fe(3\text{-}OMe\text{-}salPen)_2]ClO_4$ (**4**), and $[Fe(3\text{-}OMe\text{-}salBen)_2]ClO_4$ (**5**), where H3-OMe-salRen is the abbreviation for 2-({[2-(Ramino)ethyl]imino}methyl)-3-methoxyphenol (R = H, Me, Et, Pr, and Bu) (Chart 1), exhibit $S = 5/2$ (HS) $\rightleftharpoons$ $S = 1/2$

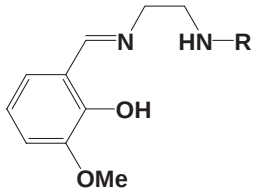

R = H, Me, Et, Pr, and Bu

Chart 1.

Published on the web March 8, 2006; DOI 10.1246/bcsj.79.442

(LS) spin transitions with thermal hysteresis. Furthermore, we report on the structures of the HS and LS states for the compounds.

Experimental

Syntheses. $[Fe(3\text{-}OMe\text{-}salHen)_2]ClO_4$ (**1**). A yellow Schiff-base solution was formed by adding 3-methoxysalicylaldehyde (0.30 g, 2 mmol) dissolved in methanol (20 mL) to a solution of ethylenediamine (0.12 g, 2 mmol) dissolved in methanol (20 mL). Then, a solution of $Fe(ClO_4)_3 \cdot nH_2O$ (0.46 g, 1 mmol) in methanol (10 mL) was added dropwise to the yellow solution, producing a dark purple solution. The dark purple solution was filtrated and the filtrate was kept 3 °C in a refrigerator. Dark purple single crystals appeared after one week. The single crystals were washed with MeOH and dried in air. The yield was 0.34 g (28.1%). Anal. Calcd for $C_{20}H_{26}O_8N_4Cl_1Fe_1$ (**1**): C, 44.34; H, 4.84; N, 10.34%. Found: C, 44.30; H, 4.81; N, 10.32%. $[Fe(3\text{-}OMe\text{-}salMen)_2]ClO_4$ (**2**). A yellow Schiff-base solution was formed by adding 3-methoxysalicylaldehyde (0.30 g, 2 mmol) dissolved in methanol (20 mL) to a solution of *N*-methylethylenediamine (0.15 g, 2 mmol) dissolved in methanol (20 mL). Then, a solution of $Fe(ClO_4)_3 \cdot nH_2O$ (0.46 g, 1 mmol) in methanol (10 mL) was added dropwise to the yellow solution, producing a dark purple solution. The solution was filtered and taken to dryness under reduced pressure at room temperature. The dark purple solid material was recrystallized from an acetone–ethanol solution. Dark purple single crystals appeared after two days. The single crystals were washed with MeOH and dried in air. The yield was 0.40 g (35.1%). Anal. Calcd for $C_{22}H_{30}O_8N_4Cl_1Fe_1$ (**2**): C, 46.37; H, 5.31; N, 9.83%. Found: C, 46.30; H, 5.82; N, 9.80%. $[Fe(3\text{-}OMe\text{-}salEen)_2]ClO_4$ (**3**). A yellow Schiff-base solution was formed by adding 3-methoxysalicylaldehyde (0.30 g, 2 mmol) dissolved in methanol (20 mL) to a solution of *N*-ethylethylenediamine (0.18 g, 2 mmol) dissolved in methanol (20 mL). Then, a solution of $Fe(ClO_4)_3 \cdot nH_2O$ (0.46 g, 1 mmol) in methanol (10 mL) was added dropwise to the yellow solution, producing a dark purple solution. The solution was filtered and taken to dryness under reduced pressure at room temperature. The dark purple solid material was recrystallized from an acetone–ethanol solution. Dark purple single crystals appeared after two days. The single crystals were washed with MeOH and dried in air. The yield was 0.43 g (36.0%). Anal. Calcd for $C_{24}H_{34}O_8N_4Cl_1Fe_1$ (**3**): C, 48.22; H, 5.73; N, 9.37%. Found: C, 48.10; H, 5.71; N, 9.34%. $[Fe(3\text{-}OMe\text{-}salPen)_2]ClO_4$ (**4**). A yellow Schiff-base solution was formed by adding 3-methoxysalicylaldehyde (0.30 g, 2 mmol) dissolved in methanol (20 mL) to a solution of *N*-propylethylenediamine (0.21 g, 2 mmol) dissolved in methanol (20 mL). Then, a solution of $Fe(ClO_4)_3 \cdot nH_2O$ (0.46 g, 1 mmol) in methanol (10 mL) was added dropwise to the yellow solution, producing a dark purple solution. The solution was filtered and taken to dryness under reduced pressure at room temperature. The dark purple solid material was recrystallized from an acetone–ethanol solution. Dark purple single crystals appeared after two days. The single crystals were washed with MeOH and dried in air. The yield was 0.38 g (30.4%). Anal. Calcd for $C_{26}H_{38}O_8N_4Cl_1Fe_1$ (**4**): C, 49.89; H, 6.12; N, 8.95%. Found: C, 49.72; H, 6.07; N, 8.87%. $[Fe(3\text{-}OMe\text{-}salBen)_2]ClO_4$ (**5**). A yellow Schiff-base solution was formed by adding 3-methoxysalicylaldehyde (0.30 g, 2 mmol) dissolved in methanol (20 mL) to a solution of *N*-butylethylenediamine (0.24 g, 2 mmol) dissolved in methanol (20 mL). Then, a solution of $Fe(ClO_4)_3 \cdot nH_2O$ (0.46 g, 1 mmol) in methanol (10 mL) was added dropwise to the yellow solution, producing a dark purple solution. The solution was filtered and taken to dryness under reduced pressure at room temperature. The dark purple solid material was recrystallized from an acetone–ethanol solution. Dark purple single crystals appeared after two days. The single crystals were washed with MeOH and dried in air. The yield was 0.35 g (26.8%). Anal. Calcd for $C_{28}H_{42}O_8N_4Cl_1Fe_1$ (**5**): C, 51.43; H, 6.47; N, 8.57%. Found: C, 51.37; H, 6.44; N, 8.57%.

Physical Measurements. The magnetic susceptibilities of the polycrystalline samples were measured by a Quantum Design MPMS5S SQUID magnetometer at 0.5 T. Temperatures were controlled over the range 5–400 K and variable temperature magnetic susceptibility measurements were carried out.

Mössbauer spectroscopy was affected by use of a constant-acceleration spectrometer (Austin Science Associates (ASA)). Data were stored in a 1024-channel pulse height analyzer, Type 5200 (Inotech, Inc.). The temperatures were monitored with a calibrated copper vs constantan thermocouple within a variable-temperature cryostat, Type ASAD-4V-(ASA). A cobalt-57 source of 10 mCi diffused into palladium foil was used for absorption measurements. Some of the spectra were fitted to a Lorentzian line shape by using a least-squares method. Isomer shifts are reported with respect to the centroid of the spectrum of iron foil enriched with ^{57}Fe.

X-ray Crystallography. Selected violet crystals of **1**–**5** were mounted on glass fibers. All measurements were made on a Rigaku RAXIS-RAPID Imaging Plate diffractometer with graphite monochromated Mo Kα radiation. The data were collected to a maximum 2θ value of 55.0°. The temperature of the crystal was slowly decreased from 298 to 90 K, and the X-ray structure analyses were carried out at 298 and 90 K. For **1** at 298 K, of the 10259 reflections that were collected, 5151 were unique and 3740 with $I > 3\sigma(I)$ were used to solve the structure with SIR92. For **1** at 90 K, of the 10453 reflections that were collected, 5017 were unique and 3607 with $I > 3\sigma(I)$ were used to solve the structure with SIR92. For **2** at 298 K, of the 20121 reflections that were collected, 5156 were unique and 3289 with $I > 3\sigma(I)$ were used to solve the structure with SIR92. For **2** at 90 K, of the 20144 reflections that were collected, 5045 were unique and 3637 with $I > 3\sigma(I)$ were used to solve the structure with SIR92. For **3** at 298 K, of the 12597 reflections that were collected, 6097 were unique and 3084 with $I > 3\sigma(I)$ were used to solve the structure with SIR92. For **3** at 90 K, of the 10855 reflections that were collected, 5678 were unique and 4419 with $I > 3\sigma(I)$ were used to solve the structure with SIR92. For **4** at 298 K, of the 8128 reflections that were collected, 5494 were unique and 1325 with $I > 3\sigma(I)$ were used to solve the structure with SIR92. For **5** at 298 K, of the 21052 reflections that were collected, 7283 were unique and 1157 with $I > 3\sigma(I)$ were used to solve the structure with SIR92. For **5** at 90 K, of the 19076 reflections that were collected, 6411 were unique and 3744 with $I > 3\sigma(I)$ were used to solve the structure with SIR92. Pertinent crystallographic parameters are summarized in Table 1. Crystallographic data have been deposited with Cambridge Crystallographic Data Centre: Deposition numbers CCDC-288051 for **1** at 298 K, CCDC-288052 for **1** at 90 K, CCDC-288053 for **2** at 298 K, CCDC-288054 for **2** at 90 K, CCDC-288055 for **3** at 298 K, CCDC-288056 for **3** at 90 K, CCDC-288057 for **4** at 298 K, CCDC-288058 for **5** at 298 K, and CCDC-288059 for **5** at 90 K. Copies of the data can be obtained free of charge via http://www.ccdc.cam.ac.uk/conts/retrieving.html (or from the Cambridge Crystallographic Data Centre, 12, Union Road, Cambridge, CB2 1EZ, UK; Fax: +44 1223 336033; e-mail: deposit@ccdc.cam.ac.uk).

Table 1. Crystal Parameters for the Compounds **1**, **2**, **3**, **4**, and **5**

Compound	**1**		**2**		**3**		**4**	**5**	
Temperature	298 K	90 K	298 K	90 K	298 K	90 K	298 K	298 K	90 K
Formula	$C_{20}H_{26}O_8N_4Cl_1Fe_1$		$C_{22}H_{30}O_8N_4Cl_1Fe_1$		$C_{24}H_{34}O_8N_4Cl_1Fe_1$		$C_{26}H_{38}O_8N_4Cl_1Fe_1$	$C_{28}H_{42}O_8N_4Cl_1Fe_1$	
Formula weight	541.75		569.80		597.85		625.91	653.96	
Crystal system	triclinic		monoclinic		triclinic		triclinic	monoclinic	
Space group	$P\bar{1}$ (#2)		$P2_1/c$ (#14)		$P\bar{1}$ (#2)		$P\bar{1}$ (#2)	$P2_1/n$ (#14)	
a/Å	9.2719(7)	9.1102(7)	11.4593(5)	11.3070(3)	10.0779(3)	9.780(1)	10.663(3)	11.068(1)	10.758(2)
b/Å	10.6629(3)	10.5381(8)	10.3806(4)	10.3252(3)	10.8704(5)	10.5932(7)	10.932(2)	25.080(3)	24.977(4)
c/Å	12.2709(7)	12.1642(7)	21.075(1)	20.9142(9)	13.9561(4)	13.941(1)	14.124(4)	12.627(1)	12.215(1)
α/°	78.963(2)	79.107(2)			75.269(6)	100.080(4)	96.27(1)		
β/°	84.160(4)	84.663(2)	91.356(2)	90.303(1)	69.258(2)	108.778(4))	105.17(1)	109.660(3)	106.880(7)
γ/°	74.915(6)	74.236(3)			77.303(4)	100.794(6)	105.126(8)		
V/Å^3	1148.0(1)	1102.6(1)	2506.2(2)	2441.6(1)	1368.51(10)	1299.5(2)	1506.0(6)	3300.6(6)	3140.8(7)
Z	2	2	4	4	2	2	2	4	4
D_{calcd}/g cm^{-3}	1.567	1.632	1.510	1.550	1.451	1.528	1.380	1.316	1.383
Ref./Para. Ratio	12.18	11.75	9.85	11.19	8.99	12.88	3.67	3.05	9.88
GOF	1.44	1.12	1.47	1.19	1.41	1.37	2.11	0.97	2.10
$R1$[a)]	0.041	0.034	0.043	0.031	0.048	0.037	0.077	0.046	0.074
R[a)]	0.075	0.064	0.066	0.047	0.080	0.062	0.128	0.075	0.130
R_w[a)]	0.105	0.084	0.112	0.089	0.114	0.096	0.167	0.088	0.189

a) $R = \sum(F_o^2 - F_c^2)/\sum F_o^2$, $R_w = \sqrt{\sum w(F_o^2 - F_c^2)}/\sum w(F_o^2)^2$, $R1 = \sum ||F_o| - |F_c||/\sum |F_o|$ for $I > 3.0\sigma(I)$.

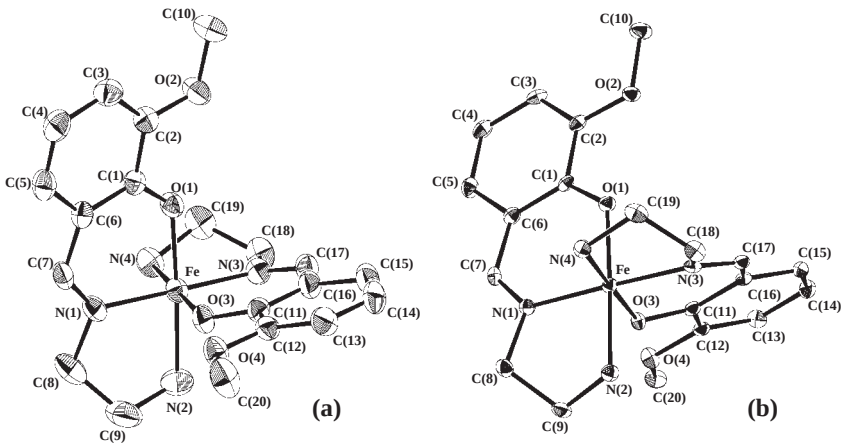

Fig. 1. ORTEP views of $[Fe(3\text{-OMe-salHen})_2]ClO_4$ (**1**) at 298 K (a) and 90 K (b) showing 50% probability displacement ellipsoids. All hydrogen atoms are omitted for clarity.

Results and Discussion

Description of Structure. The crystal structures of **1**, **2**, **3**, and **5** at 298 and 90 K, and that of **4** at 298 K, were determined by X-ray diffraction. The space groups ($P\bar{1}$ for **1**, $P2_1/c$ for **2**, $P\bar{1}$ for **3**, $P\bar{1}$ for **4**, and $P2_1/n$ for **5**) are retained upon the cooling; there is no crystallographic transition between 298 and 90 K for **1**–**5**. Figures 1–5 show the ORTEP views of the molecules together with the labeling of the atoms included in the asymmetric units for **1**–**5**, respectively.

The single-crystal X-ray analyses of **1**–**5** revealed that each of the iron(III) atoms are octahedrally coordinated by four nitrogen atoms and two oxygen atoms in two 3-OMe-salRen ligands, i.e. an N_4O_2 donor set. The Fe–O distances are shorter than the Fe–N(imine) distances, and the Fe–N(imine) distances are shorter than the Fe–N(amine) distances. Each iron atom is surrounded by two oxygen atoms and four nitrogen atoms belonging to two oxygen atoms in *cis* positions and two 3-OMe-salRen ligands. The bond lengths and angles for **1**–**5** at 298 and 90 K are listed in Tables 2 and 3. The volume of the unit cell for **3** decreases by 5.04% upon cooling from 298 to 90 K. The cell parameters a and b decrease as the temperature decreases. On the other hand, the third one, c, is constant. The volume of the unit cell for **5** decreases by 4.84% upon cooling from 298 to 90 K; the cell parameters a, b, and c decrease. However, there are no spin transitions in compounds **1**, **2**, and **4** between 298 and 90 K; **1** and **2** are in the LS state at both temperatures, and **4** is in the HS state at both temperatures.

High-Spin Crystal Structure of 3 and 5. The molecular structure of **3** at 298 K in the HS state is shown in Fig. 3a. The Fe–O and Fe–N bond lengths and the angles are sevelely distorted; the maximum difference in bond lengths is 0.31 Å between Fe–O(3) (1.911(3) Å) and Fe–N(2) (2.225(4) Å). The average values of the bond distances Fe–O (1.91 Å) and Fe–N (2.14 Å) for **3** are consistent with those for typical HS iron(III) compounds. The Fe–O distances are shorter than the Fe–N distances; this induces a pronounced distortion in the FeN_4O_2 octahedron. This is also illustrated with bond angles, O(1)–

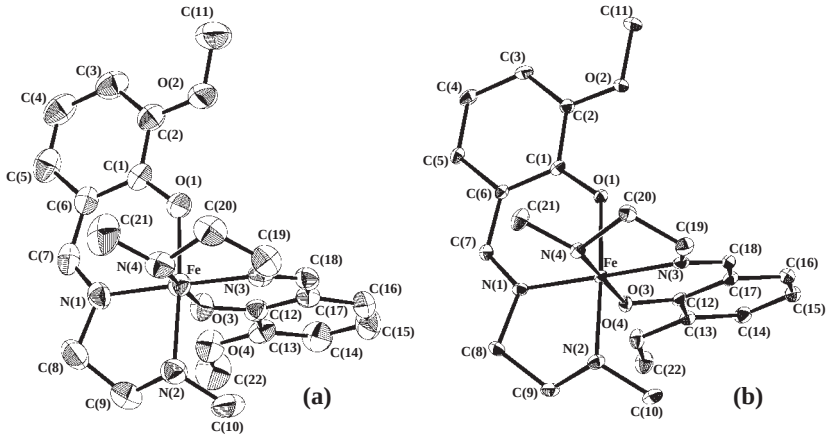

Fig. 2. ORTEP views of $[Fe(3\text{-}OMe\text{-}salMen)_2]ClO_4$ (**2**) at 298 K (a) and 90 K (b) showing 50% probability displacement ellipsoids. All hydrogen atoms are omitted for clarity.

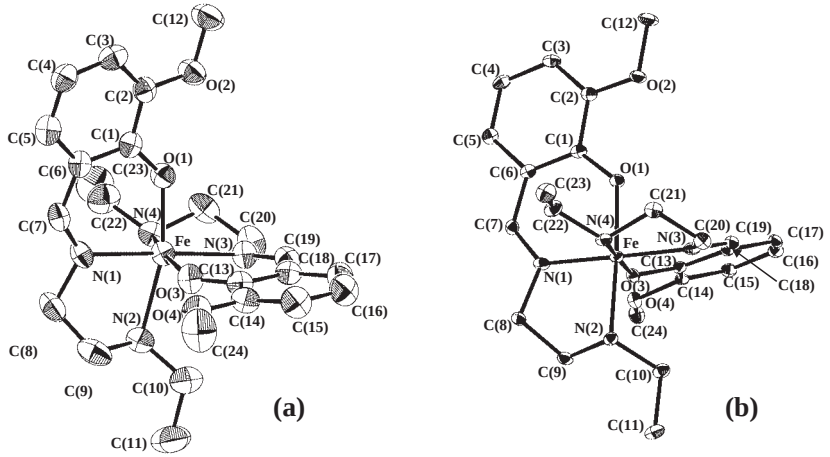

Fig. 3. ORTEP views of $[Fe(3\text{-}OMe\text{-}salEen)_2]ClO_4$ (**3**) at 298 K (a) and 90 K (b) showing 50% probability displacement ellipsoids. All hydrogen atoms are omitted for clarity.

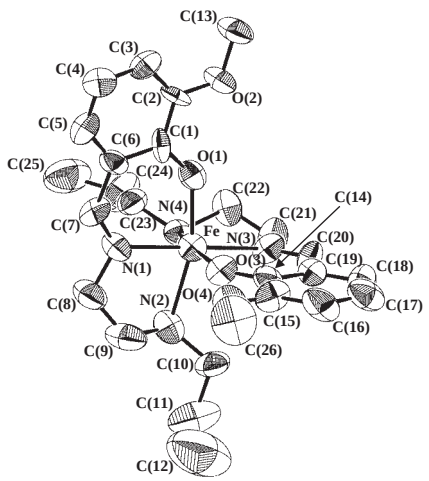

Fig. 4. ORTEP view of $[Fe(3\text{-}OMe\text{-}salPen)_2]ClO_4$ (**4**) at 298 K showing 50% probability displacement ellipsoids. All hydrogen atoms are omitted for clarity.

Fe–O(3) = 99.0(1)°, O(1)–Fe–N(2) = 165.6(1)°, O(3)–Fe–N(4) = 164.5(1)°, and N(1)–Fe–N(3) = 178.0(1)° for **3** (Table 3). The molecular structure of **5** at 298 K in the HS state is shown in Fig. 5a. The average values of the bond distances for Fe–O (1.91 Å) and Fe–N (2.14 Å) for **5** are also consistent with those for typical HS iron(III) compounds. The bond angles are illustrated by O(1)–Fe–O(3) = 96.2(3)°, O(1)–Fe–N(2) = 165.0(4)°, O(3)–Fe–N(4) = 166.9(4)°, and N(1)–Fe–N(3) = 173.0(4)° for **5** (Table 3).

Low-Spin Crystal Structure of 3 and 5. The structure of **3** at 90 K is quite similar to that at 298 K (Fig. 3b); however, the spin transition affects principally the geometry of the FeN_4O_2 core. The values of the bond distances Fe–O (1.89 Å) and Fe–N (1.99 Å) for **3** are consistent with those for typical LS iron(III) compounds. The Fe–O bonds in the LS form are shorter by 0.02 Å than those in the HS form, and the Fe–N bonds are 0.15 Å shorter than those in the HS form. The FeN_4O_2 core is less distorted in the LS state than in the HS state. The transition from HS to LS induces a decrease of 3.99° for O(1)–Fe–O(3) = 95.01°, and increase of 10.1° for O(1)–Fe–N(2) = 175.70°, 11.47° for O(3)–Fe–N(4) = 175.97° and 0.44° for N(1)–Fe–N(3) = 178.44° angles. The molecular structure of **5** at 90 K in the LS state is shown in Fig. 5b. The values of the bond distances Fe–O (1.88 Å) and Fe–N (1.99 Å) for **5** are those for typical LS iron(III) compounds. The bond angles are O(1)–Fe–O(3) = 92.8°, O(1)–Fe–N(2) = 175.9°, O(3)–

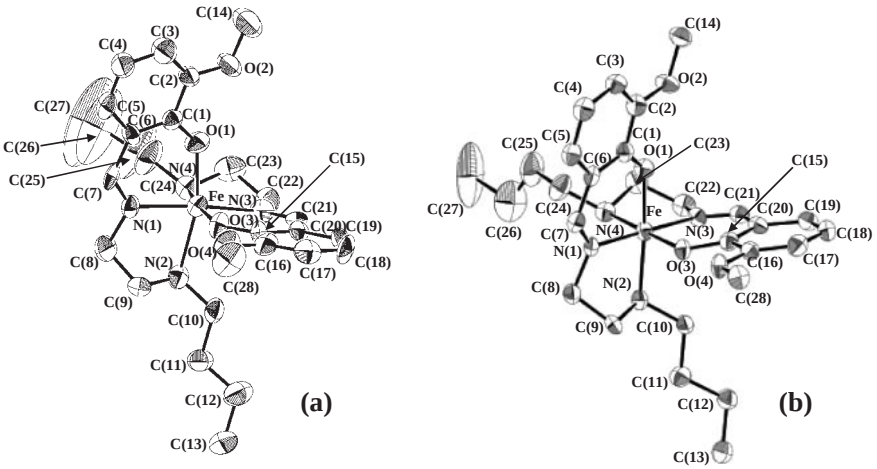

Fig. 5. ORTEP views of $[Fe(3\text{-}OMe\text{-}salBen)_2]ClO_4$ (**5**) at 298 K (a) and 90 K (b) showing 50% probability displacement ellipsoids. All hydrogen atoms are omitted for clarity.

Table 2. Selected Bond Distances (Å) and Angles (°) for Compounds **1**, **2**, and **4**

Compound	**1**		**2**		**4**
T/K	298 K	90 K	298 K	90 K	298 K
Fe–O(1)	1.874(2)	1.872(2)	1.865(2)	1.869(2)	1.96(1)
Fe–O(3)	1.880(2)	1.866(2)	1.867(2)	1.880(2)	1.95(1)
Fe–N(1)	1.923(2)	1.911(2)	1.933(3)	1.921(2)	2.10(2)
Fe–N(2)	2.022(3)	2.015(2)	2.050(3)	2.032(2)	2.25(2)
Fe–N(3)	1.922(2)	1.913(2)	1.935(3)	1.921(2)	2.13(2)
Fe–N(4)	2.030(3)	2.017(2)	2.030(3)	2.026(2)	2.22(1)
O(1)–Fe–O(3)	94.10(8)	93.85(7)	94.7(1)	94.51(8)	99.9(5)
O(1)–Fe–N(1)	92.99(9)	93.36(8)	93.3(1)	94.00(9)	86.4(5)
O(1)–Fe–N(2)	176.81(10)	177.48(7)	175.7(1)	176.46(8)	164.1(5)
O(1)–Fe–N(3)	87.00(9)	86.48(8)	87.5(1)	87.12(9)	94.2(5)
O(1)–Fe–N(4)	88.05(9)	88.00(8)	88.2(1)	87.99(8)	88.8(5)
O(3)–Fe–N(1)	87.09(9)	86.99(8)	86.0(1)	85.92(8)	94.5(5)
O(3)–Fe–N(2)	87.71(9)	87.51(8)	88.0(1)	88.14(8)	87.8(5)
O(3)–Fe–N(3)	94.14(9)	94.51(8)	93.3(1)	93.53(8)	86.1(5)
O(3)–Fe–N(4)	177.36(10)	177.84(8)	175.6(1)	176.60(9)	164.0(5)
N(1)–Fe–N(2)	84.5(1)	84.59(8)	83.6(1)	83.83(9)	79.0(6)
N(1)–Fe–N(3)	178.76(10)	178.49(8)	178.9(1)	178.78(9)	179.1(7)
N(1)–Fe–N(4)	94.33(10)	94.01(8)	97.1(1)	96.22(9)	99.5(5)
N(2)–Fe–N(3)	95.5(1)	95.53(8)	95.6(1)	95.07(9)	100.3(6)
N(2)–Fe–N(4)	90.2(1)	90.68(8)	89.2(1)	89.46(9)	87.3(5)
N(3)–Fe–N(4)	84.43(10)	84.48(8)	83.6(1)	84.28(9)	79.8(6)

Table 3. Selected Bond Distances (Å) and Angles (°) for Compounds **3** and **5**

Compound	**3**		**5**	
T/K	298 K	90 K	298 K	90 K
Fe–O(1)	1.916(3)	1.884(2)	1.915(9)	1.870(4)
Fe–O(3)	1.911(3)	1.886(2)	1.900(9)	1.883(4)
Fe–N(1)	2.071(4)	1.919(2)	2.08(1)	1.935(4)
Fe–N(2)	2.225(4)	2.062(2)	2.220(10)	2.042(5)
Fe–N(3)	2.091(4)	1.919(2)	2.07(1)	1.929(4)
Fe–N(4)	2.192(4)	2.056(2)	2.20(1)	2.057(5)
O(1)–Fe–O(3)	99.0(1)	95.01(7)	96.2(3)	92.8(2)
O(1)–Fe–N(1)	87.5(1)	93.22(8)	87.0(4)	92.8(2)
O(1)–Fe–N(2)	165.6(1)	175.70(7)	165.0(4)	175.9(2)
O(1)–Fe–N(3)	94.4(1)	85.67(7)	98.9(4)	88.2(2)
O(1)–Fe–N(4)	88.4(1)	87.57(7)	88.6(3)	87.8(2)
O(3)–Fe–N(1)	93.3(1)	86.04(7)	94.8(4)	86.3(2)
O(3)–Fe–N(2)	87.1(1)	87.39(7)	89.2(4)	89.0(2)
O(3)–Fe–N(3)	86.8(1)	92.98(7)	88.3(4)	93.9(2)
O(3)–Fe–N(4)	164.5(1)	175.97(7)	166.9(4)	177.4(2)
N(1)–Fe–N(2)	79.0(1)	83.37(8)	78.6(4)	83.6(2)
N(1)–Fe–N(3)	178.0(1)	178.44(8)	173.0(4)	179.0(2)
N(1)–Fe–N(4)	100.6(1)	96.93(8)	97.6(4)	96.2(2)
N(2)–Fe–N(3)	99.0(1)	97.79(8)	95.3(4)	95.4(2)
N(2)–Fe–N(4)	89.0(1)	90.24(7)	89.3(4)	90.5(2)
N(3)–Fe–N(4)	79.0(1)	84.11(8)	78.9(4)	83.6(2)

Fe–N(4) = 177.4°, and N(1)–Fe–N(3) = 179.0°.

Mössbauer Spectra. The variable temperature Mössbauer spectra of **1**–**5** are shown in Figs. 6–10, respectively. Typical absorptions of low-spin iron(III) ions with a large quadrupole splitting ($Q.S. = 2.659\,mm\,s^{-1}$) and a small isomer shift ($I.S. = 0.108\,mm\,s^{-1}$) were observed for the spectrum of **1** at 300 K (Fig. 6a). The spectrum of **1** at 80 K shows a quadrupole splitting of $Q.S. = 2.751\,mm\,s^{-1}$ with $I.S. = 0.171\,mm\,s^{-1}$ (Fig. 6b). The Mössbauer parameters show that the spin state for **1** is in the LS state. Two doublets (d1 and d2) were observed for **2** at 300 K (Fig. 7a). The d1 doublet has a quadrupole splitting ($Q.S. = 0.427\,mm\,s^{-1}$) and isomer shift ($I.S. = 0.152\,mm\,s^{-1}$), of which the parameters correspond to the HS state of iron(III) compounds; the d2 doublet has a quadrupole splitting ($Q.S. = 2.666\,mm\,s^{-1}$) and an isomer shift ($I.S. = 0.159\,mm\,s^{-1}$) corresponding to the LS state of iron(III) compounds. The ratio of the absorption area is HS:LS = 3:7. The spectrum of **2** at 80 K shows an asymmetric doublet and quadrupole splitting of $Q.S. = 2.908\,mm\,s^{-1}$ with $I.S. = 0.203\,mm\,s^{-1}$, corresponding to the LS state (Fig. 7b). The asymmetric doublet results from the bond anisotropy (Karyagin effect). The Mössbauer spectra show that compound **2** exhibits incomplete spin-crossover behavior between 300 and 80 K. A doublet that was observed in the Mössbauer spectrum at 300 K for **3** was assigned to the HS state of iron(III) compounds; the values of fitted parameters are $Q.S. = 0.541\,mm\,s^{-1}$ and $I.S. = 0.338\,mm\,s^{-1}$ (Fig. 8a). A doublet with $Q.S. = 2.874$ and $I.S. = 0.238\,mm\,s^{-1}$, corresponding to the LS state of iron(III)

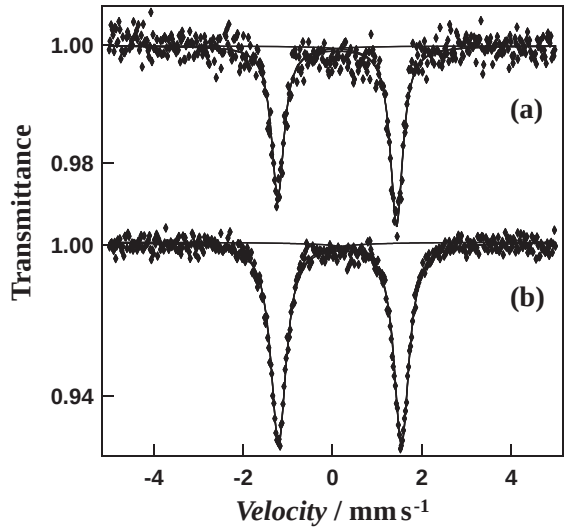

Fig. 6. Mössbauer spectra of **1** at 300 K (a) and at 80 K (b).

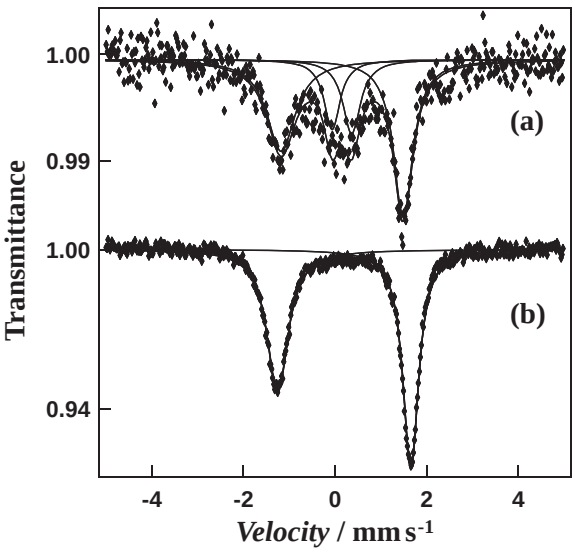

Fig. 7. Mössbauer spectra of **2** at 300 K (a) and at 80 K (b).

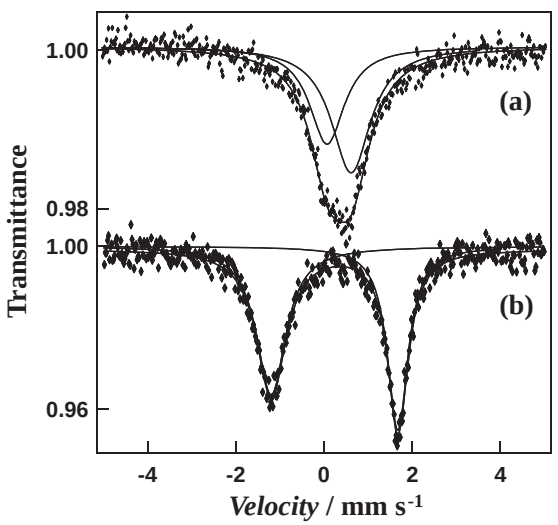

Fig. 8. Mössbauer spectra of **3** at 300 K (a) and at 80 K (b).

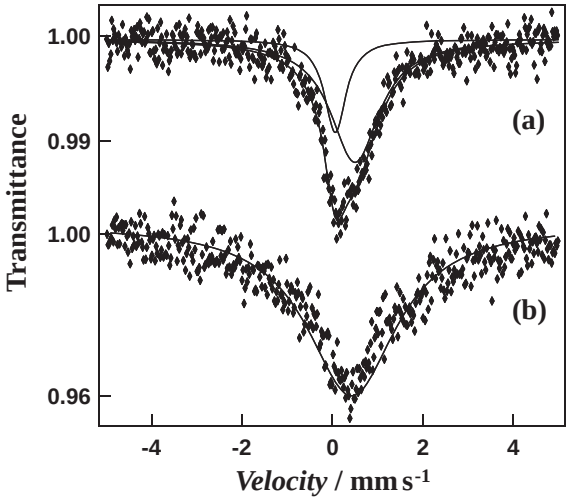

Fig. 9. Mössbauer spectra of **4** at 300 K (a) and at 80 K (b).

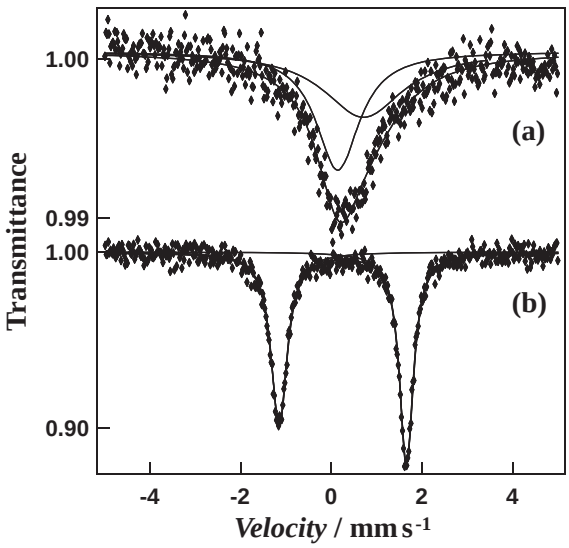

Fig. 10. Mössbauer spectra of **5** at 300 K (a) and at 80 K (b).

compounds, was observed for **3** at 80 K (Fig. 8b). The Mössbauer spectra show that compound **3** exhibits complete spin-crossover behavior between 300 and 80 K. A doublet was observed in the Mössbauer spectrum at 300 K for **4** and was assigned to the HS state of iron(III) compounds; the values of fitted parameters are $Q.S. = 0.438\,\mathrm{mm\,s^{-1}}$ and $I.S. = 0.282\,\mathrm{mm\,s^{-1}}$ (Fig. 9a). At 80 K for **4**, a broad singlet with an $I.S. = 0.427\,\mathrm{mm\,s^{-1}}$ was observed, showing that this iron(III) takes the HS state (Fig. 9b). The spectrum at 80 K is very broad and asymmetric, the exact reason for the broadening not being clear; however, spin-lattice relaxation effects on $^2T_2$ may be induced.[13] The Mössbauer parameters show that the spin state for **4** is the HS state. A doublet was observed in the Mössbauer spectrum at 300 K for **5** and was assigned to the HS state of iron(III) compounds; the values of fitted parameters are $Q.S. = 0.574\,\mathrm{mm\,s^{-1}}$ and $I.S. = 0.456\,\mathrm{mm\,s^{-1}}$ (Fig. 10a). A doublet with $Q.S. = 2.808$ and $I.S. = 0.252\,\mathrm{mm\,s^{-1}}$ corresponding to the LS state of iron(III) compounds was observed for **5** at 80 K (Fig. 10b). The Mössbauer spectra show that compound **5** exhibits complete spin-crossover behavior between 300 and 80 K.

Magnetic Susceptibilities. The temperature dependences of the magnetic susceptibility for **1**–**5** were measured in the form of the $\chi_m T$ versus T curve, where χ_m is the molar magnetic susceptibility and T is the temperature. $T_{1/2}\downarrow$ and $T_{1/2}\uparrow$ are defined as the inversion temperatures at which 50% of the molecules are in the LS and HS states in the cooling and warming modes, respectively. The $\chi_m T$ versus T plots for compounds **1**–**5** are shown in Figs. 11 and 12.

For compound **1**, $\chi_m T$ is almost constant in the 5–300 K temperature range, taking a value of around 0.45 $cm^3\,K\,mol^{-1}$ (Fig. 11). This value is consistent with the LS state ($S = 1/2$) that follows the Curie–Weiss law. The magnetic data were fitted by Eq. 1 (solid line in Fig. 11), and the Curie constant $C = 0.47\,cm^3\,K\,mol^{-1}$ and Weiss constant $\theta = 2.73$ K were obtained.

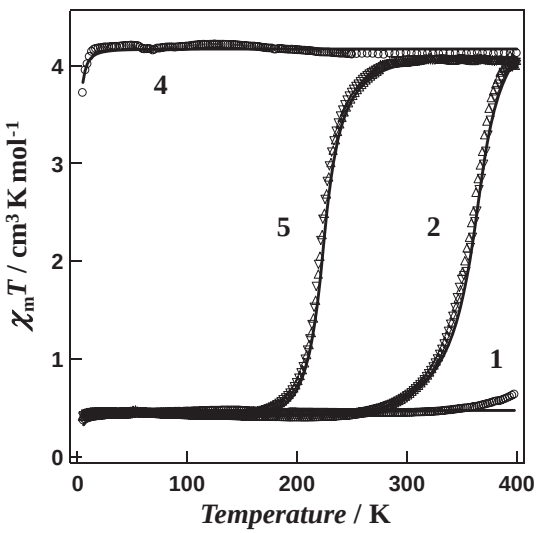

Fig. 11. Experimental and simulated $\chi_m T$ versus T plots for **1**, **2**, **4**, and **5**. The simulated curves are in full lines.

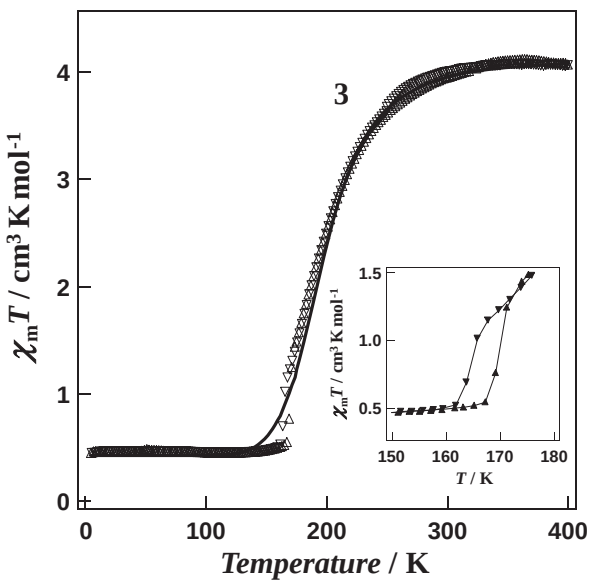

Fig. 12. Experimental and simulated $\chi_m T$ versus T plots for **3**. The simulated curves are in full lines.

$$\chi_m T = \frac{C}{T+\theta} T. \quad (1)$$

When the sample is warmed, $\chi_m T$ smoothly increases, attaining a value of 0.68 $cm^3\,K\,mol^{-1}$ at 400 K. This behavior clearly indicates the occurrence of a very incomplete (ca. 6%) $S = 5/2 \rightleftharpoons S = 1/2$ conversion at 400 K.

For compound **4**, $\chi_m T$ is equal to 4.12 $cm^3\,K\,mol^{-1}$ in the 400–20 K temperature range (Fig. 11). Then, $\chi_m T$ decreases upon cooling to 3.7 $cm^3\,K\,mol^{-1}$ at 5 K. This behavior indicates a degeneracy reduction of the ^6A_g (O_h) ground state (which splits into the ^4E and $^4A_2$ levels) resulting from the distortion. The low-temperature decrease is most likely due to zero-field splitting in the $^4A_2$ ground state. Taking this into account, we have simulated the magnetic measurements with a Hamiltonian Eq. 2:

$$\hat{H} = D[\hat{S}_z^2 - (1/3)S(S+1) + g\beta HS], \quad (2)$$

which considers an axial crystal zero-field splitting D of the ground spin state $S = 5/2$. The solid line in Fig. 11 has been obtained with the best set of parameters matching the experimental data of $|D| = 4.7\,cm^{-1}$ and $g = 1.95$. These values are reasonable and agree with those reported for other HS pseudoctahedral iron(III) compounds.[14]

The magnetic behavior of **2** displays a strong temperature dependence in the 400–250 K region, $\chi_m T = 4.01\,cm^3\,K\,mol^{-1}$ at 400 K and $\chi_m T = 0.41\,cm^3\,K\,mol^{-1}$ at 250 K, indicating the occurrence of an almost complete and relatively cooperative spin-crossover at $T_{1/2} = 360$ K (Fig. 11). The Mössbauer data do not agree with the magnetic susceptibility data because of paramagnetic impurities or differences in the detected temperatures. We have added the following; an estimate of the magnitude of the intermolecular interactions may be obtained using the mean-field model proposed by Slichter and Drickamer. In this model, the temperature dependence of γ_{HS} is given through the implicit equation Eq. 3:

$$\ln\left(\frac{1-\gamma_{HS}}{\gamma_{HS}}\right) = \frac{\Delta H + \Gamma(1-2\gamma_{HS})}{RT} - \frac{\Delta S}{R}, \quad (3)$$

where γ_{HS} is the HS molar fraction, ΔH is the value for enthalpy variations, ΔS is the value for entropy variations, and Γ is the intermolecular interaction parameter. When Γ is smaller than a threshold value equal to $2RT_{1/2}$, the transition is gradual; for $\Gamma = 2RT_{1/2}$, the transition is abrupt, but without hysteresis; $\Gamma > 2RT_{1/2}$ results in the occurrence of hysteresis. C values were defined as the cooperativity factor by $C = \Gamma/2RT_{1/2}$. Hysteresis may be observed for $C > 1$. It is possible to determine the Γ and C values by least-squares fittings of the curves of Fig. 11. The least-squares fitting leads to $\Delta H = 19.48$ $kJ\,mol^{-1}$, $\Delta S = 54.02\,J\,K^{-1}\,mol^{-1}$, and $C = 0.78$. These values are larger than those of other iron(III) compounds reported previously.[15]

The magnetic behavior of **5** also displays strong temperature dependence in the 300–150 K region, $\chi_m T = 4.04\,cm^3\,K\,mol^{-1}$ at 300 K and $\chi_m T = 0.43\,cm^3\,K\,mol^{-1}$ at 150 K, indicating the occurrence of an almost complete and relatively cooperative spin-crossover (Fig. 11). The temperature of the spin transition, $T_{1/2}$, is 223 K. The least-squares fitting for **5** leads to $\Delta H = 22.96\,kJ\,mol^{-1}$, $\Delta S = 102.86\,J\,K^{-1}\,mol^{-1}$, and $C =$

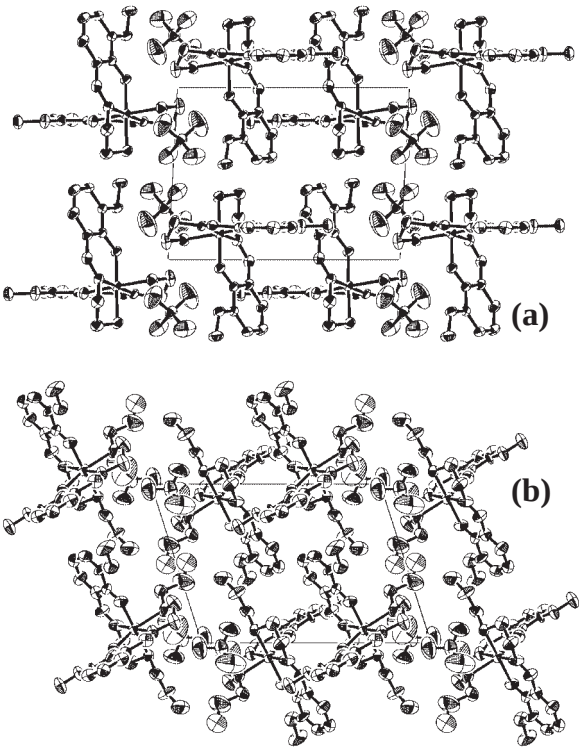

Fig. 13. (a) Crystal packing views at 298 K; (a): [Fe(3-OMe-salHen)$_2$]ClO$_4$ (**1**) and (b): [Fe(3-OMe-salPen)$_2$]-ClO$_4$ (**4**).

0.55. The value of ΔS is much greater than the electronic spin change expected for an iron(III) ion, $\Delta S_{spin} = R\ln[(2S+1)_{HS}/(2S+1)_{LS}] = 9.13\,J\,K^{-1}\,mol^{-1}$. The remaining entropy variation is mainly due to the intramolecular vibrational changes.

For compound **3**, spin-crossover behavior was observed in the temperature range from 160 to 270 K (Fig. 12). The $\chi_m T$ value at 300 K is 3.94 cm^3 K mol^{-1}, the expected value for HS iron(III) ions, and the value at 5 K is 0.45 cm^3 K mol^{-1}, the expected value for LS iron(III) ions. Moreover, a thermal hysteresis loop was observed in the temperature range from 162 to 172 K ($\Delta T = 5$ K). The magnetic curve is asymmetrical and the temperature of the spin transition, $T_{1/2}$, is 196 K. The least-squares fitting for **3** leads to $\Delta H = 12.99\,kJ\,mol^{-1}$, $\Delta S = 66.28\,J\,K^{-1}\,mol^{-1}$, and $C = 0.20$. Compound **3** has a hysteresis loop for $C < 1$ because of the asymmetrical magnetic curve. To understand the asymmetrical origin, it must be considered that the molecular interactions between HS–HS, HS–LS, and LS–LS are different. Hence, the above interpretation for the asymmetrical curves might not be a unique one, but a possible explanation. In order to investigate further the exact microscopic origin of the asymmetrical curves, additional characterization, especially the measurement of the variable temperature single-crystal structures of **3**, is required. Furthermore, the symmetry relationships and eventual symmetry breaking between the spin-crossover sites should be investigated.

Molecular Packing and Spin States. Finally, we would like to comment on the relationship between the spin states and the structures for compounds **1**–**5**. Through careful investigation of the intermolecular arrangement in the analyzed crystal structure, it was found that there are π–π or σ–π interactions between [Fe(3-OMe-salRen)$_2$]$^+$ cations. For compounds **1**, **2**, and **5**, the counter anions, ClO$_4^-$, are located between complex cations (Fig. 13a). On the other hand, two counter anions form a dimer, and the dimers are located between complex cations for **3** and **4** (Fig. 13b). The molecular arrangement for **1** shows that there are two kinds of interactions between the complex cations, i.e. π–π stacking (3.41 Å) between the phenyl ring, and CH–π interaction (2.87 Å) between the phenyl rings on an *ab* plane. The 2-D sheets extended by the interactions are bridged by perchlorate ions. This suggests that the molecular packing of **1** is very tight and **1** is in the LS state. The molecular packing of **2** shows that there are two kinds of CH–π interactions, one is between the phenyl rings (2.78 Å) and another is between the methyl substituent and phenyl ring (2.81 Å). Further, there is a weak π–π interaction (3.70 Å) between phenyl rings. As a result, compound **2** has strong interactions and exhibits spin-crossover behavior at $T_{1/2} = 360$ K. The molecular packing of **3** shows that CH–π interactions between phenyl rings (2.79 Å) and π–π stacking (3.50 Å) between phenyl rings form 2-D sheets on an *ab* plane. Furthermore, CH–π interactions between the ethyl substituent and phenyl ring (2.84 Å) exist between the 2-D sheets. This suggests that the molecular packing of **3** is very tight and **3** exhibits asymmetrical spin-crossover behavior at $T_{1/2} = 196$ K. The molecular packing of **4** shows that CH–π interactions between phenyl rings (2.81 Å), CH–π interactions between the propyl substituent and phenyl ring (2.89 Å), and π–π stacking between phenyl rings (3.44 Å) form 2-D sheets. The molecular packings for **1**–**4** are of the same style and the packing of **4** is the weakest of compounds **1**–**4**. Therefore, compound **4** does not exhibit spin-crossover and is in the HS state. The molecular packing of **5** is different from those for **1**–**4** because of the butyl substituent. The packing shows π–π stacking between the phenyl ring and CH=N moiety (3.36 Å), CH–π interactions between the butyl substituent and phenyl ring (2.84 Å), and CH–π interactions between the phenyl rings (2.86 Å) in the four complex cations. This suggests that there are strong intermolecular interactions in the molecular assembly. Compound **5** exhibits spin-crossover behavior at $T_{1/2} = 223$ K.

In summary, we have shown that iron(III) spin-crossover compounds [Fe(3-OMe-salRen)$_2$]ClO$_4$ (**1**–**5**) display various magnetic properties. The structures of compounds **1**–**5** were determined at 90 and 298 K. Compounds **2** and **5** exhibited spin-crossover behaviors without thermal hysteresis. Compound **3** exhibited asymmetrical spin-crossover behavior with thermal hysteresis. Using the mean-field model, we could simulate the spin-crossover behaviors.

This work was supported by Grant-in-Aids for Science Research (No. 17750130) from the Ministry of Education, Culture, Sports, Science and Technology of the Japanese Government.

References

1 L. Cambi, A. Cagnasso, *Atti Accad. Naz. Lincei* **1931**, *13*, 809.

2 *Spin Crossover in Transition Metal Compounds in Top. Curr. Chem.*, ed. by P. Gütlich, H. A. Goodwin, Springer, **2004**, Vol. 233–235.

3 Y. Garcìa, V. Ksenofontov, G. Levchenko, G. Schmitt, P. Gütlich, *J. Phys. Chem. B* **2000**, *104*, 5045.

4 A. Bousseksou, K. Boukheddaden, M. Goiran, C. Consejo, J. P. Tuchagues, *Phys. Rev. B* **2002**, *65*, 172412.

5 S. Decurtins, P. Gütlich, C. P. Köhler, H. Spiering, A. Hauser, *Chem. Phys. Lett.* **1984**, *105*, 1.

6 P. Gütlich, A. Hauser, H. Spiering, *Angew. Chem., Int. Ed. Engl.* **1994**, *33*, 2024.

7 S. Hayami, Z. Z. Gu, M. Shiro, Y. Einaga, A. Fujishima, O. Sato, *J. Am. Chem. Soc.* **2000**, *122*, 7126.

8 O. Kahn, J. Kröber, C. Jay, *Adv. Mater.* **1992**, *4*, 718.

9 S. Hayami, Z. Z. Gu, H. Yoshiki, A. Fujishima, O. Sato, *J. Am. Chem. Soc.* **2001**, *123*, 11644.

10 J. Kröber, E. Codjovi, O. Kahn, F. Grolière, C. Jay, *J. Am. Chem. Soc.* **1993**, *115*, 9810.

11 J.-F. Létard, P. Guionneau, E. Codjovi, O. Lavastre, G. Bravic, D. Chasseau, O. Kahn, *J. Am. Chem. Soc.* **1997**, *119*, 10861.

12 a) M. S. Haddad, M. W. Lynch, W. D. Federer, D. N. Hendrickson, *Inorg. Chem.* **1981**, *20*, 123. b) M. S. Haddad, W. D. Federer, M. W. Lynch, D. N. Hendrickson, *Inorg. Chem.* **1981**, *20*, 131. c) M. D. Timken, D. N. Hendrickson, E. Sinn, *Inorg. Chem.* **1985**, *24*, 3947.

13 a) N. Matsumoto, S. Ohta, C. Yoshimura, A. Ohyoshi, S. Kohata, H. Okawa, Y. Maeda, *J. Chem. Soc., Dalton Trans.* **1985**, 2575. b) Y. Maeda, H. Ohshio, Y. Takashima, *Chem. Lett.* **1982**, 943.

14 a) W. D. Federer, D. N. Hendrickson, *Inorg. Chem.* **1984**, *23*, 3861. b) M. D. Timken, A. M. Abdel-Mawgoud, D. N. Hendrickson, *Inorg. Chem.* **1986**, *25*, 160. c) A. J. Conti, R. K. Chadha, K. M. Sena, A. L. Rheingold, D. N. Hendrickson, *Inorg. Chem.* **1993**, *32*, 2670.

15 A. J. Conti, K. Kaji, Y. Nagano, K. M. Sena, Y. Yumoto, R. K. Chadha, A. L. Rheingold, M. Sorai, D. N. Hendrickson, *Inorg. Chem.* **1993**, *32*, 2681.